Sex Differences In Glomerular Lesions, Atherosclerosis Progression, And In The Response To Angiotensin-Converting Enzyme Inhibitors In The Apoe$^{-/-}$ Mice Model

Adrián Mallén , Ronny Rodriguez-Urquia , Rafael Alvarez , Eduard Dorca-Duch , Estanis Navarro , Miguel Hueso *

Posted Date: 13 June 2023

doi: 10.20944/preprints202306.0867.v1

Keywords: Sex differences; Chronic Kidney Disease; Atherosclerosis; Foam Cells; Parietal Epithelial Cells (PECs); Angiotensin-Converting Enzyme Inhibitors (ACEi)

Article

Sex Differences In Glomerular Lesions, Atherosclerosis Progression, And In The Response To Angiotensin-Converting Enzyme Inhibitors In The Apoe$^{-/-}$ Mice Model

Adrián Mallén [1], Ronny Rodriguez [2], Rafael Alvarez [2], Eduard Dorca-Duch [3], Estanis Navarro [1] and Miguel Hueso [1,2,*]

[1] Experimental Nephrology Lab. Institut d'Investigació Biomèdica de Bellvitge-IDIBELL, L'Hospitalet de Llobregat, Spain; amallen@idibell.cat (A.M.); estanis.navarro@gmail.com (EN); mhueso@idibell.cat (M.H).
[2] Department of Nephrology. Hospital Universitari Bellvitge, and Institutd'Investigació Biomèdica de Bellvitge-IDIBELL, L'Hospitalet de Llobregat, Spain; rrogriguez@hospitalbellvitge.cat (R.R.); ralvareze@bellvitgehospital.cat (R.A)
[3] Department of Pathology. Hospital Universitari Bellvitge. L'Hospitalet de Llobregat, Spain; edorca@bellvitgehospital.cat (E.D);
* Correspondence: mhueso@idibell.cat (M.H.); Fax: +34932607603 (M.H.); Tel.: +34932607602 (M.H.)

Abstract: This study analyzes sex-based differences in renal structure and response to the Angiotensin-Converting Enzyme (ACE) inhibitor enalapril in a mouse model of atherosclerosis. ApoE-/- mice (8 weeks old) received enalapril (5 mg/kg/day, subcutaneous) or PBS as a control for an additional 14 weeks. Each group consisted of six males and six females. Females exhibited elevated LDL-cholesterol levels, while males presented higher creatinine levels and proteinuria. Enalapril effectively reduced blood pressure in both groups, but proteinuria decreased significantly only in females. Plaque size analysis and assessment of kidney inflammation revealed no significant sex-based differences. However, males displayed more severe glomerular injury, with increased mesangial expansion, mesangiolysis, glomerular foam cells and activated parietal epithelial cells (PECs). Enalapril mitigated mesangial expansion, glomerular inflammation (particularly in females), and the hypertrophy of PECs in males. This study demonstrates sex-based differences in the response to enalapril in a mouse model of atherosclerosis. Males exhibited more severe glomerular injury, while enalapril provided renal protection, particularly in females. These findings suggest potential sex-specific considerations for ACE inhibitor therapy in chronic kidney disease and atherosclerosis cardiovascular disease. Further research is needed to elucidate the underlying mechanism behind these observations.

Keywords: Sex differences; Chronic Kidney Disease;Atherosclerosis;Foam Cells;Parietal Epithelial Cells (PECs);Angiotensin-Converting Enzyme Inhibitors (ACEi)

1. Introduction

Atherosclerosis (ATH) is the leading cause of vascular disease [1], and a growing body of evidence suggests that a decline in renal function plays a significant role in the development of ATH [2]. Furthermore, systemic hypertension, often associated with renal diseases, not only increases the risk of renal injury [3] but is also considered a modifiable risk factor for ATH [1]. One key mechanism implicated in hypertension, renal injury and ATH is angiotensin 2 (Ang2), the principal effector of the Renin-Angiotensin system (RAS) [4]. Ang2 contributes to fibrosis and inflammation, further exacerbating the damage [5] and RAS-blockage has been shown to decrease the formation and progression of atherosclerosis lesions [6] and provided renoprotection [4]. In this sense, in a mice model of ATH and reduced renal mass the administration of losartan (an AT1-R blocker) between weeks 12 and 24, reduced the development of ATH, macrophage migration and intimal infiltration [7].

 doi:10.20944/preprints202306.0867.v1

It is known that women have a lower risk for cardiovascular or CKD and show a slower progression to ESRD after an injury than men [8,9] and it has been suggested differences in responsiveness to Ang2 [10]. Thus, in a number of cardiovascular studies, women appeared to be less responsive to Angiotensin-Converting Enzyme inhibition (ACEi) than men [11,12], while proteinuric women responded better to treatment with ACEi than men [13]. Lastly, men required larger doses of AT1-R blocker to achieve the same blood pressure lowering effect than women [14].

New technologies such as the Whole Slide Imaging (WSI) that create high-resolution images, together with artificial intelligence (AI)-based slide analysis have contributed in the emergence of the digital pathology which allows a reduction in interobserver and intraobserver variability [15]. In renal pathology, AI-based automated high throughput methods using WSIs have demonstrated advantages over traditional manual reads to study the glomerulus [16,17] or for the quantification of fibrosis lesions [18].

The ApoE-/- mouse is a standard model to study ATH and has been also proposed as model of renal injury [19]. In this work, we aimed to evaluate sex-associated differences in the progression of atherosclerosis, renal disfunction, and the response to treatment with inhibitors of RAS in ApoE-/- mice, using an automated computer-assisted image analysis to obtain more precise and reproducible results.

2. Results

In the present work, mice fed with a western-style diet were treated with the RAS inhibitor, enalapril and a number of metabolic determinations and analysis were performed in males and in females with the aim to detect sex-based differences in ATH progression or treatment-related regression.

Blood lipids profile in the ApoE-/- mice model.

At the beginning of the experiment, untreated female mice presented significantly increased LDL-cholesterol levels when compared with males (25.96±8.11 mmol/L in females vs 11.45±3.96 mmol/L in males, p=0.02) but similar HDL-cholesterol (2.28±0.4 mmol/L in females vs 2.38±0.4 mmol/L in males, p=ns) or TG levels (52.28±15.89 mg/dL in females vs 84.20±21.49 mg/dL in males, p=0.5). After treatment with enalapril for 4 weeks females still presented significantly increased LDL-cholesterol (19.92±10.98 mmol/L in females vs 11.68±5.17 mmol/L in males, p=0.008) or TG levels (59.8±3 mg/dL in females vs 57.7±7.98 mg/dL in males, p=0.045), but similar HDL-cholesterol levels (2.44±0.13 mmol/L in females vs 2.64±0.14 mmol/L in males, p=ns), see also Table 1.

Table 1. Basic mice biological characteristics.

	Control	**Control**		**Enalapril**	**Enalapril**	
	Female	Male	p	Female	Male	p
n	6	6		6	6	
weight (g)	21.91 (0.58)	30.91 (1.2)	0.17	24 (3)	31 (1.9)	0.5
LDL_Cholesterol (mmol/L)	25.96 (8.11)	11.45 (3.96)	0.02	19.92 (10.98)	11.68 (5.17)	0.008
HDL_cholesterol (mmol/L)	2.28(0.45)	2.38 (0.43)	0.6	2.44 (0.13)	2.64 (0.14)	0.9
TG (mg/dL)	52.28 (15.89)	84.20 (21.49)	0.5	59.8 (3)	57.7 (7.98)	0.045
Creatinine (mg/dL)	1.1 (1.09)	4.06 (2.1)	0.012	2.04 (2.53)	1.72 (1.46)	0.5
24h Proteinuria (mg/DL)	122(58)	1122 (498)	0.016	105 (78)	1146 (290)	0.037
TAS (mmHg)	137(12)	107 (25)	0.2	108 (12)	101 (15)	0.7

Sex-related differences in blood pressure and renal function.

Male mice displayed significant higher creatinine levels (4.06±2.1 mg/dL in the male group vs 1.1±1.09 mg/dL in the female group, p=0.012) and proteinuria (1122±498 mg/dL in the male group

 doi:10.20944/preprints202306.0867.v1

vs 122±58 mg/dl in the female group, p=0.016) when compared with females, while systolic BP did not show significant variations with regard of sex (137±12 mmHg in female group vs 107±25 mmHg in male group, p=0.2). After treatment with enalapril for 4 weeks, BP was found to had lowered in both groups (108±12 mmHg in the female group vs 101±15 mmHg in the male group; p=0.7). On the other hand, creatinine showed a different evolution in both groups because its values increased in females but decreased in males (2.04±2.53 mg/dL in the female group vs 1.72±1.46 mg/dL in the male group, p=0.5), while proteinuria decreased in females but not in males (105±78 mg/dl in the female group vs 1146±290 mg/dL in the male group; p=0.003), see also Table 1.

Similar ATH in normal and enalapril-treated mice.

We did not observe significant sex-related differences on plaque size among males and females as measured with the ORO method using the sum of all the individual areas measured throughout the valve (42.22 ±7.62 % % in the female group vs 31.34±10.33% in the male group, p=0.7). Figure 1A shows a representative histologic stain on an aortic root cross-section evidencing ATH lesions. Figure 1B documents their quantification and Figure 1C measures lesions in aortas from both groups, after "en face" staining. In addition, the content of collagen in the lesions, assessed by Masson trichrome staining (TC) was also similar in both groups (38.67 ±8.99 % in the female group vs 36.34±8.18% in the male group; p=0.8). After treatment with enalapril for 4 weeks, results were similar in the two groups for lesion sizes (42.68 ±3.79 % in the female group vs 42.26±9.28% in the male group, p=0.9) or collagen content (36.16 ±8.40 % in the female group vs 43.56±8.04% in the male group, p=0.9). On the other hand, the "en face" analysis did not show significant variations among the PBS control-group (7.03 ±4.15 % in the female group vs. 11.9±4.01 % in the male group; p=0.27) or the enalapril-treated group (3.75 ±4.75 % in the female group vs. 4.11±1.30 % in the male group; p=0.71). However, differences were detected after enalapril treatment in male group (11.9±4.01 % in the male control group vs. 4.11±1.30 in the male enalapril-treated group; p=0.0029). Figure 1D shows a representative histologic stain on an aortic root cross-section evidencing collagen deposition while Figure 1E documents its quantification.

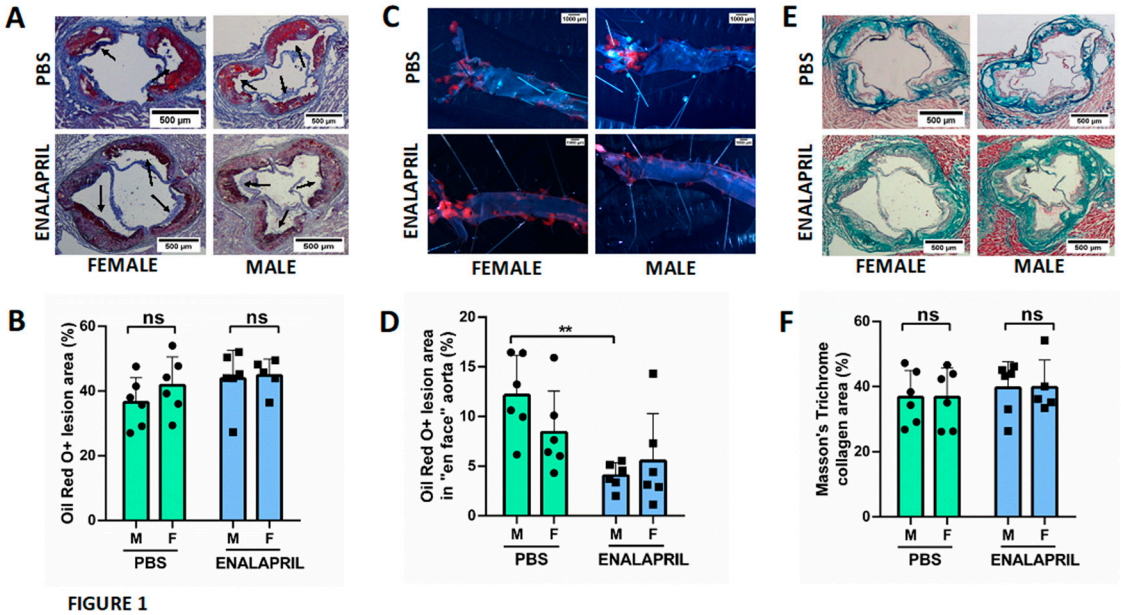

FIGURE 1

Figure 1. Treatment with enalapril does not regress atherosclerotic lesions in ApoE-deficient mice. (A) ORO staining of a representative aortic sinus of 22-week-old ApoE-/- mice female (left) or male (right) after 4 weeks of enalapril 5mg/kg/day or PBS. Scale bar = 500 m. Black arrows indicate the atherosclerotic areas (B) Lesion quantification was performed with ImageJ using the sum of all the individual areas measured throughout the valve (6-8 sections). Data are representing as mean±SEM (C) Representative en-face aortas stained with ORO. Scale bar = 1000 m. Red stains show ATH plaques (D) Quantification of the ORO positive areas of the en-face images. Enalapril reduced the

 doi:10.20944/preprints202306.0867.v1

number of plaques in ApoE-deficient males compared with the PBS group. (E) Representative aortic sinus stained with Masson's trichrome for quantification of collagen patches (in blue). Scale bar = 500 m. (F) Quantification of Collagen deposition in aortic roots was similar in all groups. Kruskall Wallis test; * P<0.01. Abbreviations: ORO: Oil Red O; M=Male; F=Female. Ns=nonsignificant; SEM=Standard error of the mean.

Male ApoE-/- mice showed increased number of glomerular foam cells and hypertrophy of PECs, while enalapril treatment reduced mesangial matrix expansion and inflammation.

Since serum creatinine and proteinuria were significantly increased in male mice, we looked for renal functional or structural alterations that could justify these results. Although, we did not find any globally sclerotic glomerulus, light microscopy revealed a number of structural findings in male mice compatible with a more severe renal injury, such as increased glomerular area (Figure 2 B) and a reduction in the urinary space in control group (26.19±0.91 % in female group vs 16.31±4% in male group, p=0.015) and enalapril treated group (32.64±2.57 % in female group vs 17.45±2.69% in male group, p<0.0001), thickening of the glomerular basement membrane, and expansion of the mesangial matrix with mesangiolysis in conjunction with the accumulation of glomerular foam cells (Figure 2 A). Nevertheless, measures of endocapilar hypercellularity (Figure 2 C) did not show significant differences among groups (1.43±0.15 % in female group vs 1.50±0.30% in male group, p=0.9). In morphological analysis, light microscopy revealed that segmental hypertrophy of parietal epithelial cells (PECs) were more prominent in males in both PBS group (0.2 ±0.13 % in female group vs 4.07±1.64% in male group, p=0.0022) and Enalapril-treated group (0.13 ±0.05 % in female group vs 4.07±1.64% in male group, p=0.0048) but differences between PBS and Enalapril groups were not significant. (Figure 2D).

 doi:10.20944/preprints202306.0867.v1

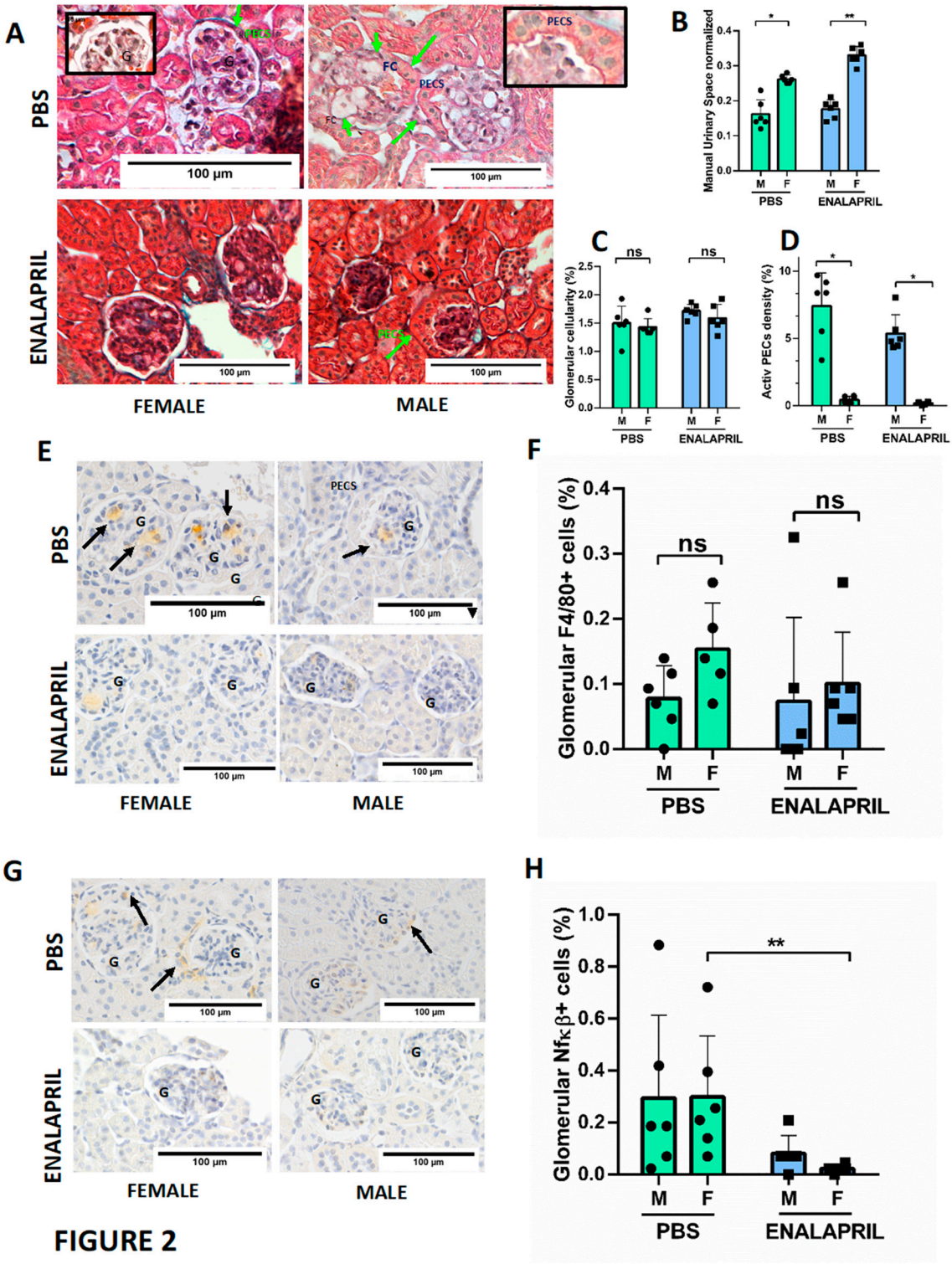

FIGURE 2

Figure 2. Glomerular injury was increased in male ApoE-/- mice. A) Representative glomerulus (G) from females (left) or males (right). Green arrows indicate urinary space (upper), while foam cells, and parietal epithelial cells are showed by letters (FC and PECS, respectively). The window in the right-upper panel shows activated PECs.(B) Quantification of the urinary space in 15 glomeruli from each mouse with ImageJ (n=6 male; n=6 female) showing its reduction in males. Scale bar = 100 m. (C) Quantification of the glomerular cellularity showed no sex-associated differences. (D) Quantification of activated PECs in glomeruli showed their increase in males. (E) Representative glomerulus showing macrophages as F4/80+ cells (black arrows). (F) Quantification of total macrophage (F4/80+ cells) infiltration. (G) Representative glomerulus showing NF-κβ+ cells (black

 doi:10.20944/preprints202306.0867.v1

arrows). (H) Quantification of NF-κβ+cells. Kruskal-Wallis was performed for statistical analyses; *P<0.01; **P<0.0001. Abbreviations: G: Glomerulus; PECs: parietal epithelial cells; M: Male; F: female.

On the other hand, and in order to evaluate the degree of inflammation in the kidney, we counted the number of glomerular infiltrating monocytes (F4/80+ cells) and the number of activated NF-kB+cells. Females showed a nonsignificant increase in infiltrating monocytes (12.79 ±8.91 % in female group vs 7.75±5.02% in male group, p=0.14) (Figure 2F) and the activation of glomerular NF-kB was also similar (29.84 ±23.46 % in female group vs 29.45±31.94 % in male group, p=0.57) as shown in Figure 2H. Tubulointerstitial damage (tubular atrophy and interstitial fibrosis) were similar (not shown). Furthermore, mice treated with ACEi enalapril showed a reduction of the mesangial matrix that increased in the urinary space, particularly in females (32.85±2.57 % in female group vs 17.46±2.69% in male group, p=0.0005). Endocapilar and mesangial hypercellularity were similar in both groups (1.59±0.24 % in female group vs 1.72±0.11% in male group, p=0.9) suggesting a reduction in glomerular pressure. In females, enalapril also reduced the number of F4/80+cells when compared with control group (12.79 ±8.91 % in controls vs 10.08 ±7.87 % in treated group, p=0.2), but not in males (7.75±5.02% in controls vs 7.36±12.86% in treated group, p=0.42). Activation of glomerular NF-kB in enalapril-treated group was reduced compared to the PBS group in both female (29.84 ±23.46 % in female control group vs 2.33 ±1.47 % in treated female group, p=0.001) and male (29.45±31.94 % in control male group vs 8.14±6.86% in treated male group, p=0.22), suggesting an improvement in the overall degree of inflammation Mice treated with enalapril also reduce the hypertrophy of PECs in male and female mice .

Lastly, we also investigated the concordance between the calculation of the glomerular area and urinary space with a deep learning software based on the MIB2 image semantic segmentation software [20]. Trained and validated network DeepLabV3 with a ResNet18 backbone and 2D U-Net architecture using QuPath 349x349x3 .tif images and .png masks (Figure 3 B), revealed good prediction of classes (global accuracy of 0.746) as showed in Figure 3D. Automatic identification of glomerular area and urinary space showed also a reduction of the urinary space in male mice in both PBS group (22.77±1.53% in female group vs 19.28±4.75% in male group, p=0.0003) and the enalapril-treated group (26.19±2.51% in female group vs 16.72±1.44%, p<0.0001) as showed in Figure 3E. The correlation graphs revealed that manual ImageJ and automatic DeepMIB2 quantification tools have a good correlation in both PBS (R=0.54) and enalapril-treated (R=0.76) groups (Figure 3 F).

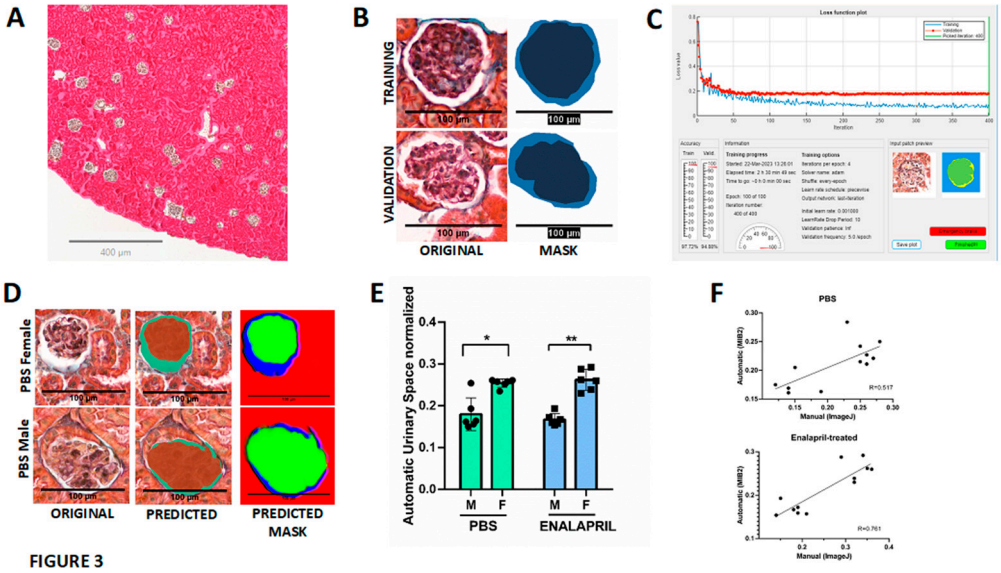

Figure 3. Examples of Deep Learning quantification of glomerular lesions. A) Representative whole slide image (WSI) used for glomerular selection in QuPath (QUP) software. Scale bar = 400 m). (B) A total number of 141 glomeruli were selected in QuPath (ORIGINAL) and 4 categories defined (urinary space, glomerulus, tuff area and exterior) to extract a mask using a QUP script (MASK). (C)

 doi:10.20944/preprints202306.0867.v1

Representative loss function plot of trained DeepMIB2 software. Blue lines in the plot showed that the system was trained and stabilized around itineration 100 (x axis) with 97.72% of accuracy while validation phase (red lines) was stabilized around 50 itineration with 94.88% of accuracy. Information about number of itineration and training progress are also shown. (D) A representative glomerulus (ORIGINAL) loaded into the DeepMIB2 trained and validated network as a test-set category for class prediction for PBS (upper images) and Enalapril-treated (lower images) groups; Scale bar = 100 m. The DeepMIB2 software predict the glomerular (brown area in the PREDICTED images) and urinary space areas (green area from PREDICTED images); Scale bar=00 m. (E) Quantification of normalized urinary space that showed a reduced reduction in males. (F) Correlation between DL method (y axis) and manual quantification with ImageJ software (x axis). Upper graph represents PBS mice group and lower graph represents enalapril-treated mice group. Kruskal-Wallis; *P<0.01; **P<0.0001. Pearson's correlation indexes (R) are shown. Abbreviations: M: Male, F: female.

3. Discussion

In this study we focused on sex-associated differences in renal function and renal morphologic alterations in kidneys from a mouse model of hypercholesterolemia and ATH since a strong link between chronic kidney diseases and atherosclerotic cardiovascular diseases (ASCVD) has been proposed. In this paper we observed a relationship between glomerular foam cell accumulation and podocyte injury in male but not in female mice. Treatment with enalapril reversed PECs hypertrophy.

It has been proposed that FSGS was analogous to atherosclerosis based on identified similarities of mesangial cells in cases of FSGS to the vascular smooth muscle-like cells that are one of the principal cell types found in atherosclerotic plaques and on the ubiquitous presence of monocyte-derived foam cells, the other major cell type found in atherosclerotic plaques [21]. These lipid-laden foam cells may be derived from a variety of cell types, including smooth muscle cells, mesangial cells, epithelial cells, endothelial cells or resident phagocytes [22], but most glomerular foam cells are derived from CD68-positive macrophages which transform into foam cells by ingesting lipids within the glomerulus “in situ” [23]. In addition, foam cells are frequently found in the interstitium in nephrotic states and in Alport syndrome and has been suggested that contribute to progressive tubulointerstitial-injury [24]. In this work, we have used ApoE-deficient mice (ApoE-/-) that develop severe hyperlipidemia due to an accumulation of chylomicrons and VLDL and lipoprotein glomerulopathy making this a model of hyperlipidemic renal injury [19] to study the impact of sex on lesion development.

The most significant finding of our study was the detection of i) increased mesangiolysis in conjunction with glomerular foam cells accumulation, and ii) swollen parietal epithelial cells (PECs) hypertrophy in male mice only, that suggest a sex predisposition to a podocyte injury and contribute to the development of FSGS. Although glomerular foam cells have been associated with extremely high levels of serum lipids, there are also glomerular foam cells not associated with hyperlipidemia in patients with FSGS [25]. These findings suggested that additional factors account for the formation of glomerular foam cells. Supporting this hypothesis, a transgenic murine model of FSGS demonstrated that an initial podocyte injury promoted lipid deposition and specific peroxidation that further produced a particular glomerular microenvironment facilitating macrophage recruitment and promoting foam cell formation at the site of injury [26]. In addition, dissolution of the normally compact mesangial matrix (“mesangiolysis”) is frequently present with glomerular foam cells accumulation, but there still remains unknown whether these processes are mechanistically linked.

To date, there has been little evidence to link glomerular foam cell accumulation to podocyte injury [22]. Currently, PECs are receiving great attention as progenitor cells of podocytes and as barrier-forming cells that prevent leaks in the periglomerular ultrafiltrate. PECs contribute to the thickening of the Bowman’s capsule basement membrane through the secretion of collagen which has been observed in diabetic nephropathy [27]. PECs also may transdifferentiate into podocytes in response to severe glomerular injury [28]. In this sense, it has been reported that hyperglycemia induce cellular hypertrophy in podocytes, mesangial cells and renal tubular cells [27]. Angiotensin converting enzyme inhibitors (ACEi) treatment demonstrated a reduction of PECs in animal models of human immunodeficiency-associated nephropathy (Tg26 mice) [29], and enhance the ability of

 doi:10.20944/preprints202306.0867.v1

PECs to turn into progenitor cells in in a model of progressive glomerular lesions in rats [30]. In our study we detected a regression in PEC hypertrophy but not in proteinuria.

FSGF has a male sex predominance and it is known that kidneys from males and females show fundamental differences in their structures [31]. Thus, the cortical proximal tubule volume density and cell height in females were 75% of that in male kidneys, but nevertheless female kidneys presented a higher proportion of collecting duct volume density and larger intercalated cells when compared with male mice [32]. Furthermore, these decreased total kidney size, proximal tubule density and proximal tubule height were reversed with testosterone replacement in a C57BL/6 mice model of orchiectomy [33]. In addition, it has been shown that the androgen receptor (AR) is expressed in both male and female kidneys, but only males showed AR in glomerular PECs [33]. Thus, in our study we observed that under stimulation only male mice present changes in the structure of the parietal lamina of Bowman Capsule that were associated with more proteinuria and poorer renal function.

The application of WSI is aimed to overcome poor intraobserver and interobserver reproducibility of scoring systems [34]. The NEPTUNE Pathology Scoring System (NPSS) provides a comprehensive scoring system by utilizing "descriptors" for patterns of glomerular and podocyte injury in each glomerulus rather than assigning conventional diagnosis to each biopsy [35]. NPSS with validated descriptors has been proposed as a model for standardization of renal biopsy interpretation [17]. In this work we used a well-established DeepLab V3 model based on a semantic segmentation CNN-based architecture with a pre-trained ResNet-18 backbone based on the Microscope Image Browser (MIB2) a high-performance MATLAB-based software for automatically identification and segmentation of glomeruli within kidney Whole Slide Imaging [36]. The DeepLab architecture employs the atrous convolutions that allows tuning the right balance between context assimilation (large field of view) and fine localization (small field of view) avoiding the loss of spatial information [37]. Our results showed a mesangial expansion due to glomerular foam cell accumulation with a clear reduction of the urinary space male mice in both PBS group and the enalapril-treated group when compared to female mice. These results were validated by two independent observers and obtained a good performance in the segmentation task with a good prediction precision. Thus, we suggest that semiautomatic or fully segmentation methods can help for a rapid and accurate characterization of glomerular lesion.

4. Materials and Methods

Reagents

In this work we used the following reagents from the stated suppliers: Enalapril (E6888-250, MG, Sigma-Merck, St Louis, MO), Angiotensin-2 (A9525-50MG; Sigma-Merck, St Louis, MO), isoflurane (PDG96236, Baxter Corporation, Illinois, USA), Hematoxilin (HHS32-1L; Sigma-Merck, St Louis, MO), Oil-Red-O (O0625; Sigma-Merck, St Louis, MO) DAB (MKCK2487, Sigma-Merck, St Louis, MO), CV Mount mounting medium (14046430011, Leica Biosystems, Wetzlar, Germany), Masson trichromacy (1004850001; Sigma-Merck, St Louis, MO), F4/80 (HM1066 Hycult Biotech, Uden, The Netherlands), anti-NF-kB (ab7970 Abcam, Cambridge, UK), Goat polyclonal antibody Vectastain ABC Kit (PK-4000, Vector laboratories, California, USA), IgG2a goat anti-rat (Novus Biological, Minnesota, USA) C57BL/6J ApoE -/- mice (Jackson Laboratories)

Mice and experimental groups

Experiments were performed in 8-week-old ApoE-/- mice on C57BL/6 background (12 males and 12 females; Jackson Laboratories, Bar Harbor, ME) fed for 10 weeks with a high fat rodent diet that contained 1.25% cholesterol and provided 40% of the energy as fat (D12108CI; Research Diets Inc, New Brunswick, NJ, USA). Mice were randomized onto three different groups, i) an enalapril group (n=12; 5 mg/kg/day enalapril dissolved in PBS and administered subcutaneously, ii) a group treated with Ang2 (n=6; 6 μg/kg/min Ang2 for 2 weeks) delivered through a subcutaneously implanted osmotic minipump (Model 1002 Micro-Osmotic Pump Alzet, Durect Corporation, Cupertino, CA,

 doi:10.20944/preprints202306.0867.v1

USA) with a pumping rate of 0.25uL/h in order to identify renal lesions caused by Ang2, and iii) a control group treated with the vehicle PBS for an additional period of 4 weeks (n=12). Animals were euthanized at 22 weeks of age by inhalation of <5% isoflurane and cardiac puncture. Next, the vascular tree was perfused with PBS under physiological pressures, and aortas and kidneys were removed, and fixed with 4% paraformaldehyde during 12h for aortas or with 10% buffered formalin during 2 days for kidneys. All animal studies were carried out in accordance with recommendations in the Guide for the care and use of Laboratory Animals of the National Institutes of Health. The protocol was approved by the Committee on the Ethics of Animal Experiments of UB-Bellvitge (number 85/20).

Blood Pressure analysis.

BP was non-invasively measured by using a tail-cuff sphygmomanometer (BP-2000 Blood Pressure Analysis System, NIBP LE5001, PANLAB) on conscious, restrained mice, before the initiation of the treatment and at the end of it. In order to reduce spontaneous variation, mice were trained for a period of 2 days to get used to the tail-cuff method. Prior to BP readings, mice were optimally warmed. All BP measures were calculated as the average of 5-measures per day.

Blood and urine analysis.

Total cholesterol, HDL, and triglyceride measurements were performed on plasma at the end of the study. 24h urine samples were collected in metabolic cages at weeks 18 and 22 of the study. Plasma creatinine and urinary concentration of protein were measured at the Clinical Veterinary Biochemistry Services of the University of Barcelona. Animals were allowed free access to water and food.

Atherosclerotic lesions analysis.

At the time of sacrifice, aortas were removed, dissected and fixed in 4% paraformaldehyde in PBS for 12h. The "en-face" area of the aortic arch and descendent aorta were cut open, pinned out flat on a black surface, and stained with Oil-Red-O (ORO). The percentage of the aortic area covered with lipid-containing plaque was measured in the whole aorta, Hearts were perfused with PBS, removed by cutting the aortic root, and further fixed in 4% paraformaldehyde in cold PBS for 12h. These were further drained and rinsed overnight in PBS containing 20% sucrose. Hearts, aortic roots and arches were embedded in OCT and tissue blocks were cut into serial 10 m-thick sections from the proximal aorta beginning at the end of the aortic sinus [38]. The composition of the plaques in the aortic root was analysed by staining with ORO and counterstaining with haematoxylin. Cryosections were stained either with Masson's trichrome staining for collagen, with anti-F4/80 antibodies to determine macrophage content, and with anti-NF-kB for inflammation. Images of each aorta were captured with a digital camera mounted on a dissection microscope. The plaque area was quantified morphometrically using the ImagePro software by measuring the extent of surface area covered by neutral lipids as revealed by ORO staining in a series of 6 sections on immediately adjacent slides that had a common anatomic location (170 m after the appearance of the 3rd valve), at the coronary ostium by calculating the percentage of ORO staining.

Renal Histology analysis.

In order to evaluate the degree of injury in kidneys sections were stained with Masson trichrome. 15 non-overlaping random field photomicrographs were acquired per sample with the Nikon Epifluorescence microscope (E800) with 40X magnification and imported into ProgRes Capture (Jenoptik, Jena, Germany). The Bowman capsule area (BA) was defined as the area of the inner side of the glomerular parietal epithelial cell layers and the glomerular area (GA) was defined as the area of the outer capillary loops of the tuft [39]. The proportion of urinary space (US) was calculated as US=BA-GA/BA. Number of nuclei, the BA, and GA were manually quantified for each glomerular cross-section from a total of 15 glomeruli using the ImageJ2 v 2.9.0/1.53t software. Each glomerulus

 doi:10.20944/preprints202306.0867.v1

was evaluated for the presence of foam cells and for histopathologic changes in parietal epithelial cells (PECs). We discriminate between quiescent and activated PECS internally lining the Bowman's capsule by morphological analysis. Quiescent PECs were flat, and activated PECS have enlarged nuclei and increased cuboidal cytoplasm [40] . The numerical density of activated PECs in glomerulus (Nv(P/Glom)) was calculated by dividing absolute PEC number per glomerulus (Q(P)) by the area of glomerular cross-sections (A(Glom)), according to the formula: Nv(P/Glom) = (Q(P)/ h x A(Glom)) x fs3, where h=1.5 was the dissector height and fs3=0.95 the linear tissue shrinkage correction factor (for Epon-embedded murine kidney tissue) [41]. Interlobular artery injury was determined by analyzing wall thickness after tracing the inner and outer circumferences of the vessel. The size of the vessel was normalized by calculating the ratio of median wall area dimension to the area of outer circumference. All the measures were done blindly by two investigators. Alternatively, for automatic and reliable identification of glomerular area and urinary space we obtained a whole slide image (WSI), from Masson's trichrome stained samples using 3d Histech P250 scanner, at 40x magnification and transformed into monofocal by using Extended Depth of Focus. A total number of 141 glomeruli were selected and 4 categories were defined manually as "annotations" (urinary space, glomeruli, tuff area and exterior) and a mask extracted by using the QuPath (QUP) v.0.4.2 software. Each glomerulus was identified and delimitated with tiles of 349 x 349 pixels and manual segmentation of Urinary space was performed using the "wand" tool. Masks and original images were split into the raining group (n=91) and validation group (n=50) and processed using a deep learning semantic segmentation algorithm that classifies every pixel in an image following the code-free approach proposed by Pettersen et al in the microscopy image segmentation software DeepMIB2 [42]. Briefly, tile images and masks were exported, in .tif and .png file formats respectively to train the DeepLabV3Resnet18 network, a convolutional network (CNN) for semantic segmentation, using the DeepMIB2 v 1.302.0.0 (Microscopy Image Browser 2) software (http://mib.helsinki.fi/). The training step encompassed 100 number of epochs, 4 iterations, a total of 141 images (adding data augmentation such as flips, rotations among others), using 0.25 fraction of validation and 16 mini-Batch size.

Kidney sections were also stained with anti-F4/80 (1/50) to study the number of interstitial macrophages and with an anti-NF-kB (1/1000) in order to evaluate inflammation in the kidney. Appropriate secondary antibodies IgG2a goat anti-rat (1/100) and Goat polyclonal antibody Vectastain ABC Kit (1/200), were used before DAB development. Finally, sections were counterstained with Harris hematoxylin and covered with CV Mount mounting medium. Number of F4/80 or NF-K -positive cells were quantified in 43 glomeruli. Fluorescence intensity was graded by using a semiquantitative scale from 0 (negative) to 4 (very strong). For all histological analysis, simultaneous negative control staining reactions were performed without the primary antibody. The results represent the percentage of glomeruli that contained positive cells.

Statistical analysis

Data were expressed as mean±SD. Blood pressure changes, biochemistry parameters and the extension of atherosclerosis and renal lesions were determined using the nonparametric Mann-Whitney or Kruskal-Wallis Test. The level of significance was $P<0.05$. Statistics were performed with R version 4.1.3 (2022-03-10).

5. Conclusions

In conclusion, in this work we show that males from the ApoE model of ATH displayed a more severe glomerular injury than females with an increased accumulation of glomerular foam cells and activation of parietal epithelial cells (PECs), both suggesting a functional link among lipid metabolism, podocyte injury and sex hormones. Treatment with Enalapril offered renal protection particularly in females, as well as the normalization of PECs function.

Author Contributions: Conceptualization, AM, EN and MH; Methodology, AM, ED, EN and MH; Validation: ED, EN; Formal Analysis: AM, RR, RA, ED, EN, and MH; Investigation: AM, RR, RA, ED, EN, MH; Resources,

ED, MH; Data Curation, AM, RR, RA, ED, EN and MH; Writing-Original Draft Preparation, AM, EN and MH; Visualization, AM, ED, and MH; Supervision, EN and MH; Project Administration, AM, EN and MH; Funding Acquisition, MH.

Funding: This study has been partially funded by Instituto de Salud Carlos III (Co-funded by European Regional Development Fund. ERDF, a way to build Europe) through the project PI 18/01108 to MH and by RICORS (RD21/0005/0001). We thank the CERCA program/Generalitat de Catalunya for institutional support.

Institutional Review Board Statement: The animal study protocol was approved by the Ethics Committee of of Animal Experiments of UB-Bellvitge (number 85/20, FUE-2021-01925942 and NRB0ZCGZG, aproved 18.03.2022).

Data Availability Statement: The data generated during this study are available upon request.

Acknowledgments: We thank the CERCA program/Generalitat de Catalunya for institutional support.

Conflicts of Interest: The authors declare no conflict of interest.

References

1. Herrington, W., B. Lacey, P. Sherliker, J. Armitage, and S. Lewington. "Epidemiology of Atherosclerosis and the Potential to Reduce the Global Burden of Atherothrombotic Disease." Circ Res 118, no. 4 (Feb 19 2016): 535-46. https://dx.doi.org/10.1161/CIRCRESAHA.115.307611.
2. Kon, V., M. F. Linton, and S. Fazio. "Atherosclerosis in Chronic Kidney Disease: The Role of Macrophages." Nat Rev Nephrol 7, no. 1 (Jan 2011): 45-54. https://dx.doi.org/10.1038/nrneph.2010.157.
3. Griffin, K. A. "Hypertensive Kidney Injury and the Progression of Chronic Kidney Disease." Hypertension 70, no. 4 (Oct 2017): 687-94. https://dx.doi.org/10.1161/HYPERTENSIONAHA.117.08314.
4. Mori, T., and A. W. Cowley. "Role of Pressure in Angiotensin Ii-Induced Renal Injury: Chronic Servo-Control of Renal Perfusion Pressure in Rats." Hypertension 43, no. 4 (Apr 2004): 752-9. https://dx.doi.org/10.1161/01.HYP.0000120971.49659.6a.
5. Long, D. A., K. L. Price, J. Herrera-Acosta, and R. J. Johnson. "How Does Angiotensin Ii Cause Renal Injury?", Hypertension 43, no. 4 (Apr 2004): 722-3. https://dx.doi.org/10.1161/01.HYP.0000120964.22281.3e.
6. Silva, G. M., M. S. França-Falcão, N. T. M. Calzerra, M. S. Luz, D. D. A. Gadelha, C. M. Balarini, and T. M. Queiroz. "Role of Renin-Angiotensin System Components in Atherosclerosis: Focus on Ang-Ii, Ace2, and Ang-1-7." Front Physiol 11 (2020): 1067. https://dx.doi.org/10.3389/fphys.2020.01067.
7. Suganuma, E., Y. Zuo, N. Ayabe, J. Ma, V. R. Babaev, M. F. Linton, S. Fazio, I. Ichikawa, A. B. Fogo, and V. Kon. "Antiatherogenic Effects of Angiotensin Receptor Antagonism in Mild Renal Dysfunction." J Am Soc Nephrol 17, no. 2 (Feb 2006): 433-41. https://dx.doi.org/10.1681/ASN.2005080883.
8. Man, J. J., J. A. Beckman, and I. Z. Jaffe. "Sex as a Biological Variable in Atherosclerosis." Circ Res 126, no. 9 (Apr 24 2020): 1297-319. https://dx.doi.org/10.1161/CIRCRESAHA.120.315930.
9. Bairey Merz, C. N., L. M. Dember, J. R. Ingelfinger, A. Vinson, J. Neugarten, K. L. Sandberg, J. C. Sullivan, C. Maric-Bilkan, T. L. Rankin, P. L. Kimmel, R. A. Star, and participants of the National Institute of Diabetes and Digestive and Kidney Diseases Workshop on "Sex and the Kidneys". "Sex and the Kidneys: Current Understanding and Research Opportunities." Nat Rev Nephrol 15, no. 12 (Dec 2019): 776-83. https://dx.doi.org/10.1038/s41581-019-0208-6.
10. Hilliard, L. M., E. S. Jones, U. M. Steckelings, T. Unger, R. E. Widdop, and K. M. Denton. "Sex-Specific Influence of Angiotensin Type 2 Receptor Stimulation on Renal Function: A Novel Therapeutic Target for Hypertension." Hypertension 59, no. 2 (Feb 2012): 409-14. https://dx.doi.org/10.1161/HYPERTENSIONAHA.111.184986.
11. Falconnet, C., M. Bochud, P. Bovet, M. Maillard, and M. Burnier. "Gender Difference in the Response to an Angiotensin-Converting Enzyme Inhibitor and a Diuretic in Hypertensive Patients of African Descent." J Hypertens 22, no. 6 (Jun 2004): 1213-20. https://dx.doi.org/10.1097/00004872-200406000-00023.
12. Hudson, M., E. Rahme, H. Behlouli, R. Sheppard, and L. Pilote. "Sex Differences in the Effectiveness of Angiotensin Receptor Blockers and Angiotensin Converting Enzyme Inhibitors in Patients with Congestive Heart Failure--a Population Study." Eur J Heart Fail 9, no. 6-7 (2007): 602-9. https://dx.doi.org/10.1016/j.ejheart.2007.02.001.
13. Ruggenenti, P., A. Perna, C. Zoccali, G. Gherardi, R. Benini, A. Testa, and G. Remuzzi. "Chronic Proteinuric Nephropathies. Ii. Outcomes and Response to Treatment in a Prospective Cohort of 352 Patients: Differences between Women and Men in Relation to the Ace Gene Polymorphism. Gruppo Italiano Di Studi Epidemologici in Nefrologia (Gisen)." J Am Soc Nephrol 11, no. 1 (Jan 2000): 88-96. https://dx.doi.org/10.1681/ASN.V11188.
14. Miller, J. A., D. Z. Cherney, J. A. Duncan, V. Lai, K. D. Burns, C. R. Kennedy, J. Zimpelmann, W. Gao, D. C. Cattran, and J. W. Scholey. "Gender Differences in the Renal Response to Renin-Angiotensin System Blockade." J Am Soc Nephrol 17, no. 9 (Sep 2006): 2554-60. https://dx.doi.org/10.1681/ASN.2005101095.

15. Wu, B., and G. Moeckel. "Application of Digital Pathology and Machine Learning in the Liver, Kidney and Lung Diseases." J Pathol Inform 14 (2023): 100184. https://dx.doi.org/10.1016/j.jpi.2022.100184.
16. Rosenberg, A. Z., M. Palmer, L. Merlino, J. P. Troost, A. Gasim, S. Bagnasco, C. Avila-Casado, D. Johnstone, J. B. Hodgin, C. Conway, B. W. Gillespie, C. C. Nast, L. Barisoni, and S. M. Hewitt. "The Application of Digital Pathology to Improve Accuracy in Glomerular Enumeration in Renal Biopsies." PLoS One 11, no. 6 (2016): e0156441. https://dx.doi.org/10.1371/journal.pone.0156441.
17. Barisoni, L., J. P. Troost, C. Nast, S. Bagnasco, C. Avila-Casado, J. Hodgin, M. Palmer, A. Rosenberg, A. Gasim, C. Liensziewski, L. Merlino, H. P. Chien, A. Chang, S. M. Meehan, J. Gaut, P. Song, L. Holzman, D. Gibson, M. Kretzler, B. W. Gillespie, and S. M. Hewitt. "Reproducibility of the Neptune Descriptor-Based Scoring System on Whole-Slide Images and Histologic and Ultrastructural Digital Images." Mod Pathol 29, no. 7 (Jul 2016): 671-84. https://dx.doi.org/10.1038/modpathol.2016.58.
18. Sánchez-Jaramillo, E. A., L. E. Gasca-Lozano, J. M. Vera-Cruz, L. D. Hernández-Ortega, and A. M. Salazar-Montes. "Automated Computer-Assisted Image Analysis for the Fast Quantification of Kidney Fibrosis." Biology (Basel) 11, no. 8 (Aug 17 2022). https://dx.doi.org/10.3390/biology11081227.
19. Wen, M., S. Segerer, M. Dantas, P. A. Brown, K. L. Hudkins, T. Goodpaster, E. Kirk, R. C. LeBoeuf, and C. E. Alpers. "Renal Injury in Apolipoprotein E-Deficient Mice." Lab Invest 82, no. 8 (Aug 2002): 999-1006. https://dx.doi.org/10.1097/01.lab.0000022222.03120.d4.
20. Belevich, I., and E. Jokitalo. "Deepmib: User-Friendly and Open-Source Software for Training of Deep Learning Network for Biological Image Segmentation." PLoS Comput Biol 17, no. 3 (Mar 2021): e1008374. https://dx.doi.org/10.1371/journal.pcbi.1008374.
21. Diamond, J. R., and M. J. Karnovsky. "Focal and Segmental Glomerulosclerosis: Analogies to Atherosclerosis." Kidney Int 33, no. 5 (May 1988): 917-24. https://dx.doi.org/10.1038/ki.1988.87.
22. Eom, M., K. L. Hudkins, and C. E. Alpers. "Foam Cells and the Pathogenesis of Kidney Disease." Curr Opin Nephrol Hypertens 24, no. 3 (May 2015): 245-51. https://dx.doi.org/10.1097/MNH.0000000000000112.
23. Saito, T., T. Ootaka, H. Sato, T. Furuta, T. Sato, J. Soma, K. Abe, and K. Yoshinaga. "Participation of Macrophages in Segmental Endocapillary Proliferation Preceding Focal Glomerular Sclerosis." J Pathol 170, no. 2 (Jun 1993): 179-85. https://dx.doi.org/10.1002/path.1711700214.
24. Wu, Y., Y. Chen, D. Chen, C. Zeng, L. Li, and Z. Liu. "Presence of Foam Cells in Kidney Interstitium Is Associated with Progression of Renal Injury in Patients with Glomerular Diseases." Nephron Clin Pract 113, no. 3 (2009): c155-61. https://dx.doi.org/10.1159/000232596
25. Stokes, M. B., A. M. Valeri, G. S. Markowitz, and V. D. D'Agati. "Cellular Focal Segmental Glomerulosclerosis: Clinical and Pathologic Features." Kidney Int 70, no. 10 (Nov 2006): 1783-92. https://dx.doi.org/10.1038/sj.ki.5001903.
26. Hara, S., N. Kobayashi, K. Sakamoto, T. Ueno, S. Manabe, Y. Takashima, J. Hamada, I. Pastan, A. Fukamizu, T. Matsusaka, and M. Nagata. "Podocyte Injury-Driven Lipid Peroxidation Accelerates the Infiltration of Glomerular Foam Cells in Focal Segmental Glomerulosclerosis." Am J Pathol 185, no. 8 (Aug 2015): 2118-31. https://dx.doi.org/10.1016/j.ajpath.2015.04.007.
27. Kawaguchi, T., K. Hasegawa, I. Yasuda, H. Muraoka, H. Umino, H. Tokuyama, A. Hashiguchi, S. Wakino, and H. Itoh. "Diabetic Condition Induces Hypertrophy and Vacuolization in Glomerular Parietal Epithelial Cells." Sci Rep 11, no. 1 (Jan 15 2021): 1515. https://dx.doi.org/10.1038/s41598-021-81027-8.
28. Gaut, J. P., M. Hoshi, S. Jain, and H. Liapis. "Claudin 1 and Nephrin Label Cellular Crescents in Diabetic Glomerulosclerosis." Hum Pathol 45, no. 3 (Mar 2014): 628-35. https://dx.doi.org/10.1016/j.humpath.2013.10.030.
29. Yadav, A., S. Vallabu, D. Kumar, G. Ding, D. N. Charney, P. N. Chander, and P. C. Singhal. "Hivan Phenotype: Consequence of Epithelial Mesenchymal Transdifferentiation." Am J Physiol Renal Physiol 298, no. 3 (Mar 2010): F734-44. https://dx.doi.org/10.1152/ajprenal.00415.2009.
30. Benigni, A., M. Morigi, P. Rizzo, E. Gagliardini, C. Rota, M. Abbate, S. Ghezzi, A. Remuzzi, and G. Remuzzi. "Inhibiting Angiotensin-Converting Enzyme Promotes Renal Repair by Limiting Progenitor Cell Proliferation and Restoring the Glomerular Architecture." Am J Pathol 179, no. 2 (Aug 2011): 628-38. https://dx.doi.org/10.1016/j.ajpath.2011.04.003.
31. Beckwith, H., L. Lightstone, and S. McAdoo. "Sex and Gender in Glomerular Disease." Semin Nephrol 42, no. 2 (Mar 2022): 185-96. https://dx.doi.org/10.1016/j.semnephrol.2022.04.008.
32. Harris, A. N., H. W. Lee, G. Osis, L. Fang, K. L. Webster, J. W. Verlander, and I. D. Weiner. "Differences in Renal Ammonia Metabolism in Male and Female Kidney." Am J Physiol Renal Physiol 315, no. 2 (Aug 01 2018): F211-F22. https://dx.doi.org/10.1152/ajprenal.00084.2018.
33. Harris, A. N., H. W. Lee, J. W. Verlander, and I. D. Weiner. "Testosterone Modulates Renal Ammonia Metabolism." Am J Physiol Renal Physiol 318, no. 4 (Apr 01 2020): F922-F35. https://dx.doi.org/10.1152/ajprenal.00560.2019.
34. Ozluk, Y., P. L. Blanco, M. Mengel, K. Solez, P. F. Halloran, and B. Sis. "Superiority of Virtual Microscopy Versus Light Microscopy in Transplantation Pathology." Clin Transplant 26, no. 2 (2012): 336-44. https://dx.doi.org/10.1111/j.1399-0012.2011.01506.x.

35. Barisoni, L., C. C. Nast, J. C. Jennette, J. B. Hodgin, A. M. Herzenberg, K. V. Lemley, C. M. Conway, J. B. Kopp, M. Kretzler, C. Lienczewski, C. Avila-Casado, S. Bagnasco, S. Sethi, J. Tomaszewski, A. H. Gasim, and S. M. Hewitt. "Digital Pathology Evaluation in the Multicenter Nephrotic Syndrome Study Network (Neptune)." Clin J Am Soc Nephrol 8, no. 8 (Aug 2013): 1449-59. https://dx.doi.org/10.2215/CJN.08370812.
36. Jha, A., H. Yang, R. Deng, M. E. Kapp, A. B. Fogo, and Y. Huo. "Instance Segmentation for Whole Slide Imaging: End-to-End or Detect-Then-Segment." J Med Imaging (Bellingham) 8, no. 1 (Jan 2021): 014001. https://dx.doi.org/10.1117/1.JMI.8.1.014001
37. Chen, L. C., G. Papandreou, I. Kokkinos, K. Murphy, and A. L. Yuille. "Deeplab: Semantic Image Segmentation with Deep Convolutional Nets, Atrous Convolution, and Fully Connected Crfs." IEEE Trans Pattern Anal Mach Intell 40, no. 4 (Apr 2018): 834-48. https://dx.doi.org/10.1109/TPAMI.2017.2699184.
38. Hueso, M., A. Mallén, E. Ripoll, L. de Ramón, N. Bolaños, C. Varela, J. Guiteras, J. Checa, E. Navarro, J. M. Grinyo, J. M. Cruzado, J. M. Aran, and J. Torras. "Cd40 Silencing by Sirna Infusion in Rodents and Evaluation by Kidney Immunostaining." Bio Protoc 11, no. 10 (May 20 2021): e4032. https://dx.doi.org/10.21769/BioProtoc.4032.
39. Sasaki, T., N. Tsuboi, K. Haruhara, Y. Okabayashi, G. Kanzaki, K. Koike, A. Kobayashi, I. Yamamoto, M. Ogura, and T. Yokoo. "Bowman Capsule Volume and Related Factors in Adults with Normal Renal Function." Kidney Int Rep 3, no. 2 (Mar 2018): 314-20. https://dx.doi.org/10.1016/j.ekir.2017.10.007.
40. Su, H., S. Chen, F. F. He, Y. M. Wang, P. Bondzie, and C. Zhang. "New Insights into Glomerular Parietal Epithelial Cell Activation and Its Signaling Pathways in Glomerular Diseases." Biomed Res Int 2015 (2015): 318935. https://dx.doi.org/10.1155/2015/318935.
41. Herbach, N., I. Schairer, A. Blutke, S. Kautz, A. Siebert, B. Göke, E. Wolf, and R. Wanke. "Diabetic Kidney Lesions of Giprdn Transgenic Mice: Podocyte Hypertrophy and Thickening of the Gbm Precede Glomerular Hypertrophy and Glomerulosclerosis." Am J Physiol Renal Physiol 296, no. 4 (Apr 2009): F819-29. https://dx.doi.org/10.1152/ajprenal.90665.2008.
42. Pettersen HS, Belevich I, Røyset ES, Smistad E, Simpson MR, Jokitalo E, Reinertsen I, Bakke I, Pedersen A. Code-Free Development and Deployment of Deep Segmentation Models for Digital Pathology. Front Med (Lausanne). 2022 Jan 27;8:816281. doi: 10.3389/fmed.2021.816281. PMID: 35155486; PMCID: PMC8829033